Evaluation of Capacity Spectrum Methods for Seismic Fragility Analysis of Bridges

교량의 지진 취약도 해석 시 사용되는 성능 스펙트럼 기법의 평가

김 상 훈* 이 진 학** 김 호 경***
Kim, Sang Hoon Yi, Jin Hak Kim, Ho Kyung

국문요약

본 연구는 콘크리트 교량의 지진취약도 곡선을 개발함에 있어 성능 스펙트럼 기법(Capacity Spectrum Method)에 대한 고찰을 통해 가장 적절한 해석방법을 제시하는데 그 목적이 있다. 원래 성능 스펙트럼 기법은 빌딩 구조물을 위한 간략화된 정적 비선형 해석의 일환으로 개발되었는 바, 본 연구에서는 이 기법을 교량의 지진취약도 곡선을 개발하는데 응용하였다. 서로 다른 네가지의 방법으로 성능 스펙트럼 기법을 통해 구해진 취약도 곡선들을 비선형 시간이력해석 방법에 의해 구해진 취약도 곡선과 비교하였다. 취약도 곡선은 두 개의 변수를 가진 lognormal 분포를 따르는 것으로 가정하였으며 PGA(Peak Ground Acceleration)의 함수로 나타내어졌다. FEMA(Federal Emergency Management Agency) SAC(SEAOC-ATC-CUREe) steel 프로젝트에 의해 개발된 로스앤젤레스 지역 60개의 지진이 교량해석을 위해 사용되었다. 성능 스펙트럼 기법과 시간이력해석에 따라 만들어진 교량의 지진취약도 곡선들을 비교 검토한 바, 이 중 하나의 방법이 부합되는 결과를 보여주었다. 요구 스펙트럼 작성시 본 논문에서 제시된 지침을 따르면 비선형 시간이력 해석시와 유사한 결과를 얻을 수 있을 것으로 사료된다. 다만 지진과 교량이 지닌 특수성으로 인해 본 연구의 결과가 항상 적용되는지는 더 심도있는 연구를 통해 검증되어야 할 것이다.

주요어 : 비선형 정적해석, 성능스펙트럼기법, 취약도 곡선, 연성계수, Pushover 해석, 비선형 시간이력해석

ABSTRACT

This study presents the evaluation of CSM(Capacity Spectrum Method, ATC-40) in developing fragility curves for a sample concrete bridge. The CSM is originally developed as one of the simplified procedures for building structures, while this study adopts the CSM to develop fragility curves of bridge structures. Four(4) different approaches are demonstrated and the fragility curves developed are compared those by the nonlinear time history analysis. Fragility curves in this study are represented by lognormal distribution functions with two parameters and developed as a function of PGA. The sixty(60) ground acceleration time histories for the Los Angeles area developed for the Federal Emergency Management Agency (FEMA) SAC(SEAOC-ATC-CUREe) steel project are used for the bridge analysis. The comparison of fragility curves by the CSM with those by the time history analysis indicates that the agreement is excellent for one of the methods investigated in this study. In this respect, it is recommended that the demand spectrum might be improved according to the guidelines suggested in this study. However, this observation might not always apply, depending on the details of specific bridge characteristic

Key words : nonlinear static procedure, capacity spectrum method, fragility curve, ductility, pushover analysis, nonlinear time history analysis

1. Introduction

In general, complete nonlinear time history analysis has been perceived as the most reliable method in performing seismic risk analysis of a structure with seismic vulnerability of its components identified for various states of damages. The vulnerability information can be taken into consideration most conveniently in the form of fragility curves as widely practiced. This rigorous analysis, however, would be a time consuming procedure and would leave something desired to reflect engineering intuition and physical understanding.

Several recent studies[1]-[3] have successfully demonstrated that similar concepts and procedures in the nonlinear static procedure[4] originally developed for building structures can be also applied to bridge structures for performance-based seismic evaluation under certain reasonable conditions. ATC-40[4] states "Available nonlinear static procedures include (1) the capacity spectrum method(CSM)(e.g., ATC-40)[4] that uses the intersection of the capacity(or pushover) curve and a reduced response spectrum to estimate maximum displacement; (2) the displacement coefficient method(e.g., FEMA-273)[5] that uses pushover analysis and a modified version of the equal displacement approximation to estimate maximum displacement; and (3) the secant method(e.g., City of Los Angeles, Division 95)[6] that uses a substitute structure and secant stiffness".

This study focuses on the CSM to develop the fragility curves as a function of PGA(Peak Ground Acceleration) for the sample bridge under the ground acceleration time histories assuming that the fragility curves can be expressed in the form of two-parameter log-normal distribution functions. Four(4) different demand spectrums are considered to

* (주)대우건설 토목기술팀 차장, 공학박사(대표저자 : ksh1210@chol.com)
** 한국과학기술원 스마트 사회기반시설 연구센터, 연구조교수, 공학박사
*** 국립목포대학교 토목전공 부교수, 공학박사
본 논문에 대한 토의를 2004년 4월 30일까지 학회로 보내 주시면 그 결과를 게재하겠습니다. (논문접수일 : 2003. 12. 29 / 심사종료일 : 2004. 2. 5)

utilize CSM and the results are compared with those from the nonlinear time history analysis. This study provides insightful information on the seismic evaluation on bridges for pre- and post-earthquake events as well as the seismic design.

2. Bridge Models and Seismic Ground Motion

2.1 Description of Bridges

A sample bridge in California is selected for example analysis with the elevation and the column section shown in Fig. 1. The bridge has the overall length of 34m with three spans. The superstructure consists of a longitudinally reinforced concrete deck slab 10m wide and it is supported by two pairs of columns(and by an abutment at each end). Each pair has three columns of circular cross section with 0.76m diameter.

A column is modeled as an elastic zone with a pair of plastic zones at each end of the column. Each plastic zone is then modeled to consist of a nonlinear rotational spring and a rigid element depicted in Fig. 2. The plastic hinge formed in the bridge column is assumed to have bilinear hysterestic characteristics. Springs are also attached to the bases of the columns to account for soil effects, while two abutments are modeled as roller supports. To reflect the cracked state of a concrete bridge column for the seismic response analysis, an effective moment of inertia is employed, making the period of the bridge correspondingly longer.

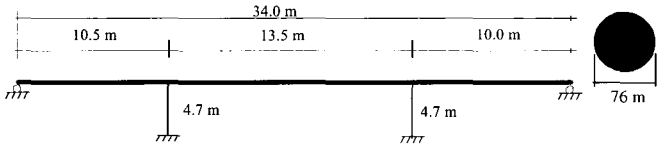

Fig. 1 Elevation and column section of sample bridge

2.2 Moment-Curvature Curves and Damage States

Evaluation of nonlinear response of the bridge arising from the column nonlinearity is based on moment-curvature curve analysis taking axial loads as well as confinement effects into account. The moment-curvature relationship used in this study for the nonlinear spring is bilinear without any stiffness degradation. Its parameters are established using the COLx computer code developed by Caltrans.[7]

The critical parameter used to describe the nonlinear structural response in this study is the ductility demand. The ductility demand is defined as $\mu = \theta / \theta_y$, where θ is the rotation of a bridge column at its plastic hinge and θ_y is the corresponding rotation at the yield point.

A set of five (5) different damage states are also introduced following the Dutta[1] recommendations. Table 1 displays the description of these five damage states and the corresponding drift limits for a typical column. For each limit state, the drift limit can be transformed to peak ductility demand of the columns for the purpose of this study. Table 2 lists the corresponding values for the sample bridge.

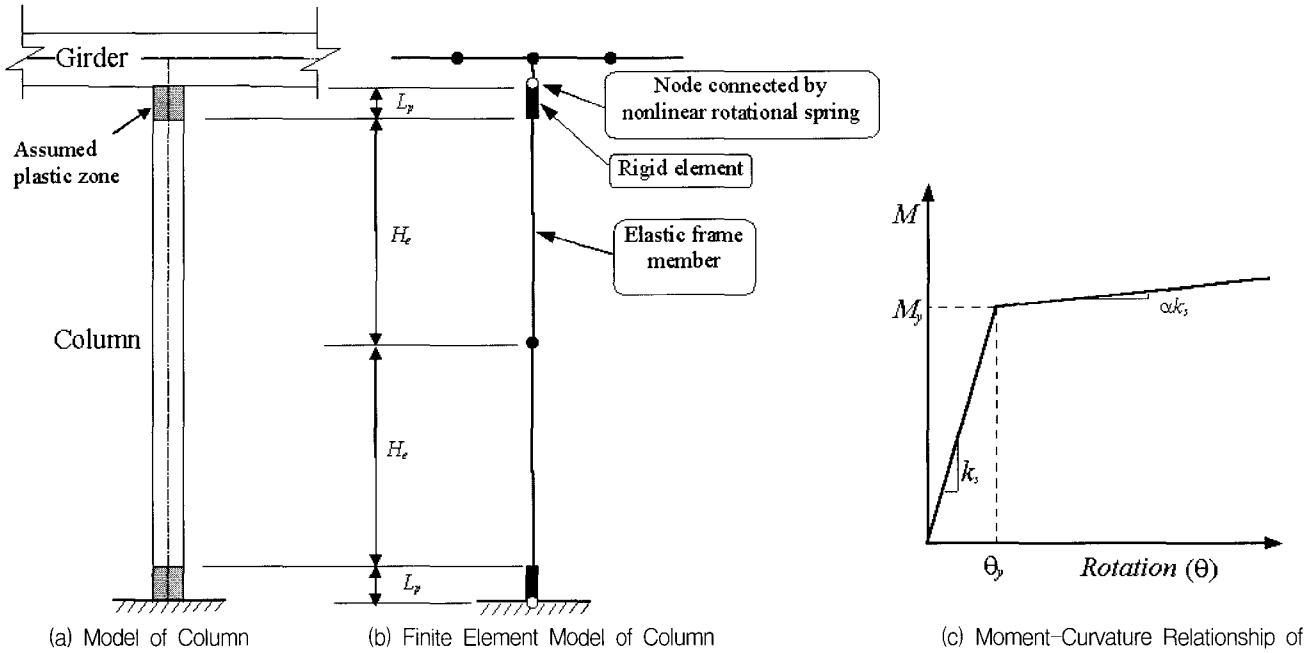

(a) Model of Column (b) Finite Element Model of Column (c) Moment-Curvature Relationship of Nonlinear Rotational Spring

Fig. 2 Nonlinear model for the bridge column

Table 1 Description of damage states

Damage state	Description	Drift limits
Almost no	First yield	0.005
Slight	Cracking, spalling	0.007
Moderate	Loss of anchorage	0.015
Extensive	Incipient column collapse	0.025
Complete	Column collapse	0.05

Table 2 Peak ductility demand of column of sample bridge

Damage states	ductility demand
Almost no	$1.00 < \mu < 1.34$
Slight	$1.34 < \mu < 2.71$
Moderate	$2.71 < \mu < 4.42$
Extensive	$4.42 < \mu < 8.70$
Complete	$8.70 < \mu$

2.3 Seismic Ground Motion

The sixty(60) ground acceleration time histories for the Los Angeles area developed for the Federal Emergency Management Agency(FEMA) SAC(SEAOC-ATC-CUREe) steel project are used for the bridge analysis to develop the fragility curves. These acceleration time histories are derived from historical records with some linear adjustments and consist of three(3) groups(each consisting of 20 time histories) having probabilities of exceedence of 10% in 50 years, 2% in 50 years and 50% in 50 years respectively, as listed in Table 3.

These sixty(60) Los Angeles earthquake time histories are grouped and scaled to their PGA representative values listed in Table 4 for the purpose of applying CSM to develop fragility curves. It should be noted that the scaling of ground motions to a specific PGA value might change the characteristics of the earthquake ground motions resulting in different responses of structures. This change, however, is considered to be disregardable in approximation

3. Capacity Spectrum Method(CSM)

The terms "Demand" and "Capacity" are two key elements in using the CSM. The "Demand" represents intensity of the seismic ground motion to which bridges are subjected and the "Capacity" represents the bridges' ability to resist the seismic demand, while two(2) primary spectrums (Capacity Spectrum and Demand Spectrum) are also required to determine a performance point during the procedure of CSM. These are utilized conforming to ATC-40[4] and the procedure developed by Shinozuka et al[3] is

Table 3 Description of Los Angeles Ground Motions

10% Exceedence in 50 yr				2% Exceedence in 50 yr				50% Exceedence in 50 yr			
SAC Name	DT (sec)	Duration (sec)	PGA (cm/sec^2)	SAC Name	DT (sec)	Duration (sec)	PGA (cm/sec^2)	SAC Name	DT (sec)	Duration (sec)	PGA (cm/sec^2)
LA01	0.02	39.4	452	LA21	0.02	60.0	1258	LA41	0.01	39.4	578
LA02	0.02	39.4	663	LA22	0.02	60.0	903	LA42	0.01	39.4	327
LA03	0.01	39.4	386	LA23	0.01	25.0	410	LA43	0.01	39.1	141
LA04	0.01	39.4	479	LA24	0.01	25.0	464	LA44	0.01	39.1	110
LA05	0.01	39.4	296	LA25	0.005	15.0	852	LA45	0.02	78.6	142
LA06	0.01	39.4	230	LA26	0.005	15.0	925	LA46	0.02	78.6	156
LA07	0.02	80.0	413	LA27	0.02	60.0	909	LA47	0.02	80.0	331
LA08	0.02	80.0	418	LA28	0.02	60.0	1304	LA48	0.02	80.0	302
LA09	0.02	80.0	510	LA29	0.02	50.0	794	LA49	0.02	60.0	312
LA10	0.02	80.0	353	LA30	0.02	50.0	973	LA50	0.02	60.0	536
LA11	0.02	39.4	653	LA31	0.01	30.0	1271	LA51	0.02	44.0	766
LA12	0.02	39.4	951	LA32	0.01	30.0	1164	LA52	0.02	44.0	619
LA13	0.02	60.0	665	LA33	0.01	30.0	767	LA53	0.02	26.1	680
LA14	0.02	60.0	645	LA34	0.01	30.0	668	LA54	0.02	26.1	775
LA15	0.005	15.0	523	LA35	0.01	30.0	973	LA55	0.02	60.0	508
LA16	0.005	15.0	569	LA36	0.01	30.0	1079	LA56	0.02	60.0	372
LA17	0.02	60.0	558	LA37	0.02	60.0	698	LA57	0.02	79.5	248
LA18	0.02	60.0	801	LA38	0.02	60.0	761	LA58	0.02	79.5	227
LA19	0.02	60.0	999	LA39	0.02	60.0	491	LA59	0.02	40.0	754
LA20	0.02	60.0	968	LA40	0.02	60.0	613	LA60	0.02	40.0	469

Table 4 Grouping and Scaling of PGA values

Representative PGA	Ground motion names (PGA values)	Number of data
0.2g	la44(0.1117), la43(0.1435), la45(0.1444), la46(0.1592), la58(0.2312), la6(0.2348), la57(0.2532)	7
0.4g	la5(0.3017), la48(0.3079), la49(0.3188), la42(0.3335), la47(0.3380), la10(0.3606), la56(0.3792), la3(0.3939), la23(0.4183), la7(0.4214), la8(0.4260), la1(0.4613), la24(0.4732), la60(0.4786), la4(0.4884)	15
0.6g	la39(0.5006), la55(0.5179), la9(0.5201), la15(0.5340), la50(0.5468), la17(0.5698), la16(0.5802), la41(0.5901), la40(0.6258), la52(0.6320), la14(0.6576), la11(0.6658), la2(0.6764), la13(0.6785), la34(0.6812), la53(0.6939)	16
0.8g	la37(0.7121), la59(0.7691), la38(0.7768), la51(0.7813), la33(0.7829), la54(0.7909), la29(0.8096), la18(0.8178), la25(0.8690)	9
1.0g	la22(0.9212), la27(0.9272), la26(0.9442), la12(0.9703), la20(0.9874), la30(0.9924), la35(0.9930), la19(1.0198), la36(1.1013), la32(1.1872)	10
1.2g	la21(1.2837), la31(1.2971), la28(1.3307)	3

introduced below using the sample bridge and the seismic ground motion time histories described in the previous section.

3.1 Capacity Spectrum

A capacity beyond the elastic limits for a structural frame is determined by performing the pushover analysis. In order to plot the force-displacement curve, the total shear force at column bottoms is tracked as a function of displacement of the superstructure. The lateral forces are applied in proportion to the fundamental mode shape as shown in Fig. 3 below where F_i is the lateral force on node i($i=1,2,\cdots N$), w_i dead weight assigned to node i, ϕ_i amplitude of the fundamental mode at node i, V the base shear and the number of nodes.[3]

$$F_i=\left(w_i\phi_i/\sum_{i=1}^{N}w_i\phi_i\right)V \tag{1}$$

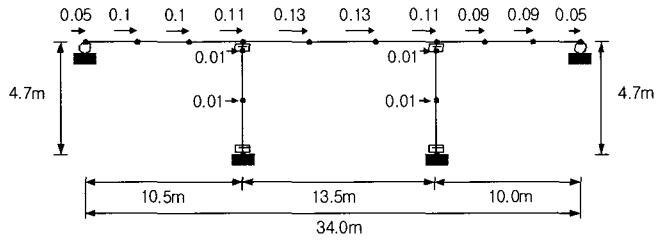

Fig. 3 Applied load pattern to the fundamental mode of bridge model

By increasing lateral loads(or base shear) gradually as shown in Fig. 4, plastic hinges are formed in succession at column bottoms and overall pushover curve deviates from the initial straight line for elastic deformation as shown in Fig. 5.

To utilize CSM, it is necessary to transform the capacity curve to the capacity spectrum. The capacity curve expresses overall shear force on all supports as a function of the horizontal displacement of the superstructure, while the capacity spectrum represents the capacity curve in the ADRS (Acceleration-Displacement Response Spectra) format. The spectral acceleration S_a and the spectral displacement S_d can be obtained using the following equations[4];

$$S_a=\frac{V/W}{\alpha} \tag{2}$$

$$S_d=\frac{\Delta_{girder}}{PF\phi_{girder}}=\frac{\theta_{pl}}{PF\phi_{pl}} \tag{3}$$

where V is base shear, W overall dead weight of bridge, α modal participation factor, Δ_{girder} horizontal displacement of girder, θ_{pl} rotation of plastic hinge, ϕ_{girder} and ϕ_{pl} amplitudes of the fundamental mode at girder and plastic hinge, PF respectively, modal participation factor of the fundamental mode defined as follows.

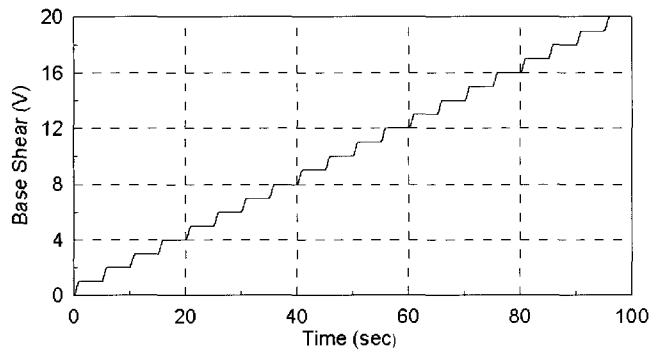

Fig. 4 Base shear increments with respect to time

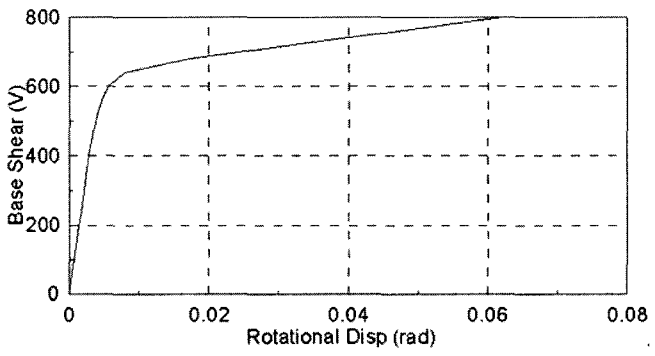

Fig. 5 Capacity curve derived from pushover analysis

$$PF=\left[\frac{\sum_{i=1}^{N}(w_i\phi_i)/g}{\sum_{i=1}^{N}(w_i\phi_i^2)/g}\right] \tag{4}$$

$$\alpha=\frac{\left[\sum_{i=1}^{N}(w_i\phi_i)/g\right]^2}{\left[\sum_{i=1}^{N}w_i/g\right]\left[\sum_{i=1}^{N}(w_i\phi_i^2)/g\right]} \tag{5}$$

The spectral displacement S_d can be calculated at any displacement component of the structure as shown in (3). Although the horizontal displacement of girder is considered as a most critical displacement component for developing the capacity curve for building structures, the rotation of plastic hinge is more conveniently used to develop the capacity curve for bridge structures when the rotational ductility demand of plastic hinge at column bottom is used to represent the damage states defined in the previous section. Fig. 6 shows capacity spectrum developed for the sample bridge.

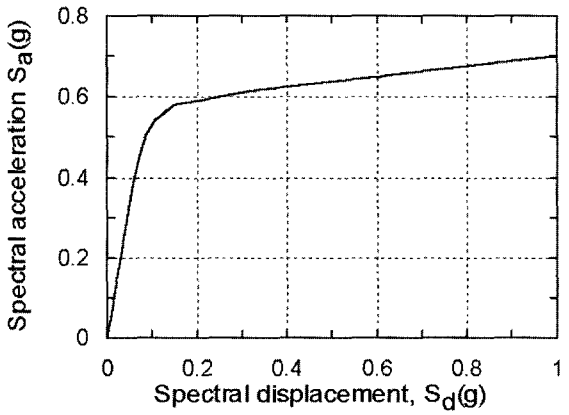

Fig. 6 Capacity spectrum

3.2 Demand Spectrum

Standard elastic acceleration response spectrum can be transformed to ADRS format using the following Eq. (4).

$$S_d=\frac{T^2}{4\pi^2}S_a g \tag{6}$$

According to ATC-40[4], the reduced inelastic ADRS is developed by multiplying the reduction factors SR_A and SR_V for the range of constant spectral peak acceleration and constant spectral peak velocity, respectively as follows;

$$SR_A=\frac{3.21-0.68\ln(\beta_{eff})}{2.12}\geq \text{values in Table 5} \tag{7}$$

$$SR_A=\frac{2.31-0.41\ln(\beta_{eff})}{2.12}\geq \text{values in Table 6} \tag{8}$$

where β_{eff}(in percentage) is the effective viscous damping including assumed 5% structural damping as follows;

$$\beta_{eff}=\kappa\beta_0+5=\frac{63.7\kappa(a_y d_{pi}-d_y a_{pi})}{a_{pi}d_{pi}}+5 \tag{9}$$

where β_0 is equivalent viscous damping associated with full hysteresis loop area of capacity spectrum, κ is damping modification factor to compensate for the uncertainty in β_0 because of probable imperfections in real bridge hysteresis loops and defined as a function of structural behavior type as shown in Table 6. Also, in (9), (d_y, a_y) represents the yielding point on the bilinear capacity spectrum, and (d_{pi}, a_{pi}) the performance point on the bilinear capacity spectrum at the i^{th} trial with the significance of yield points and performance points graphically depicted later in Figs. 7 and 8. It should be mentioned that the selection of structural behavior type affects the response of bridge in connection with two parameters such as the "minimum allowable values of reduction factors" in Table 5 and the "damping modification factor", κ in Table 6. Both parameters play an important role in determining the spectral reduction factors, SR_A and SR_V. Assuming that any probable imperfection in real bridge hysteresis loops is not considered in time history analysis, SR_A and SR_V in (7) and (8) can be obtained without reducing β_0 with κ (i.e., $\kappa=1.0$) in (9) and without limiting by the minimum allowable values in Table 5. The structural behavior type A is also considered to be the most reasonable assumption in this study. But this case may overestimate the effective damping resulting in overly reduced response.

Table 5 Minimum allowable SR_A and SR_V values[4]

Structural behavior type	SR_A	SR_V
Type A	0.33	0.50
Type B	0.44	0.56
Type C	0.56	0.67

Table 6 Values for damping modification factor, κ[4]

Structural behavior type	β_0	κ
Type A	≤16.25	1.0
	>16.25	$1.13-0.008\beta_0\geq 0.77$
Type B	≤25	0.67
	>25	$0.845-0.007\beta_0\geq 0.53$
Type C	any value	0.33

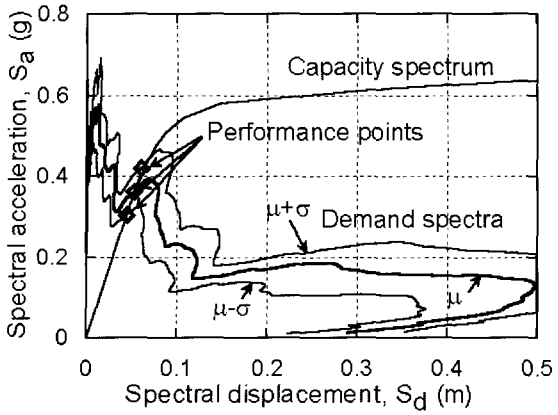

(a) Representative PGA=0.2g

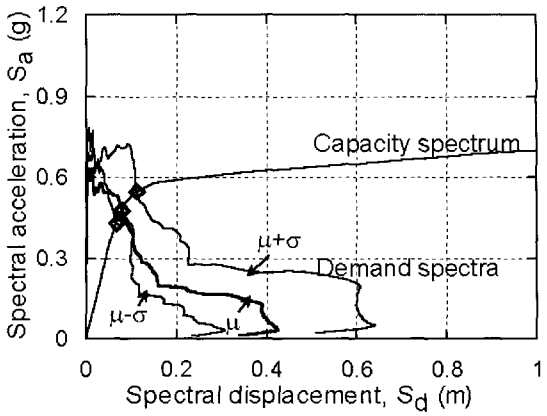

(b) Representative PGA=0.4g

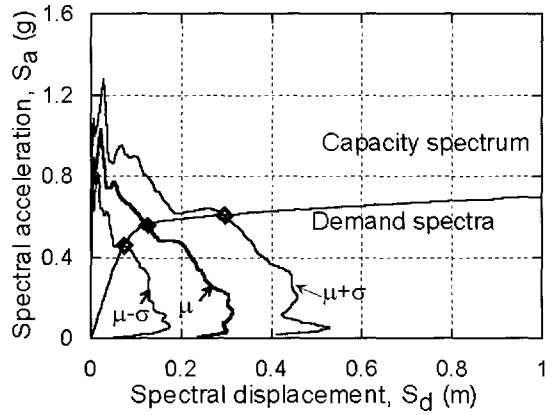

(c) Representative PGA=0.6g

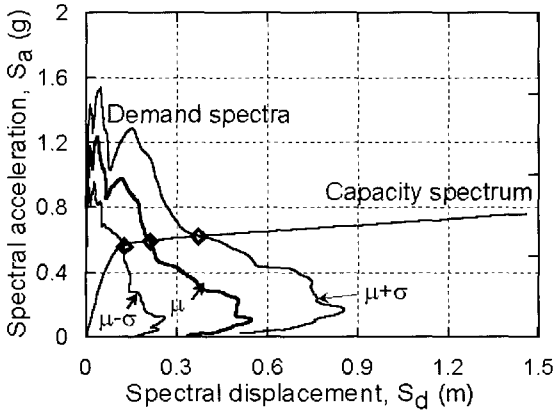

(d) Representative PGA=0.8g

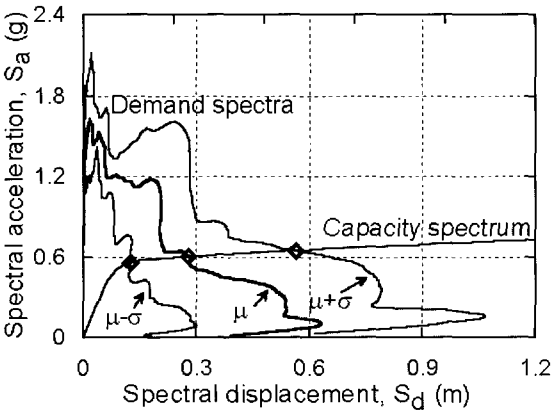

(e) Representative PGA=1.0g

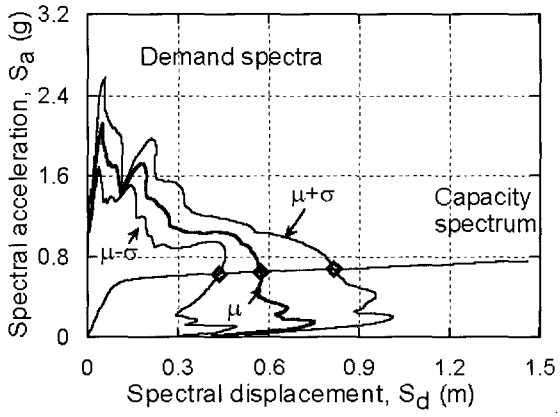

(f) Representative PGA=1.2g

Fig. 7 ADRS for time histories grouped to representative PGA(CSM1)

3.3 Performance Point

In determining a performance point, it is assumed that when the displacement d_{pi} at the intersection of the reduced demand spectrum with the ±5 capacity spectrum falls within the percent range of the displacement of the performance point obtained at $(i\text{-}1)^{th}$ iteration i.e., $(0.95_{p(i-1)} \leq d_{pi} \leq 1.05_{p(i-1)}$, d_{pi} becomes the performance point.

4. Development of Fragility Curve

4.1 Fragility Curves by Time History Analysis

In this study, the fragility curves are expressed in the form of two-parameter lognormal distribution functions, and the two parameters(median and log-standard deviation) are estimated with the aid of the maximum likelihood method. A common log-standard deviation, which forces

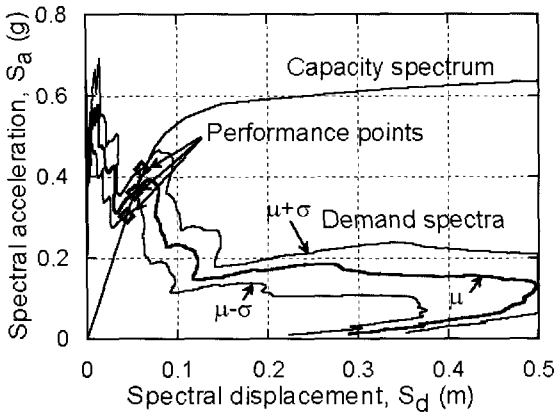

(a) Representative PGA=0.2g

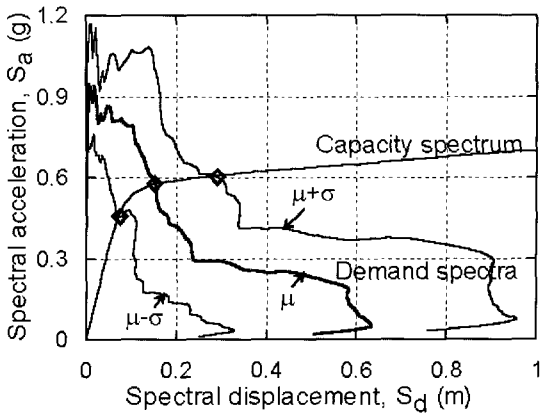

(b) Representative PGA=0.4g

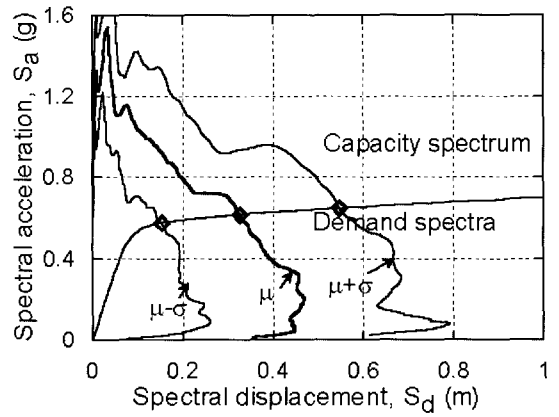

(c) Representative PGA=0.6g

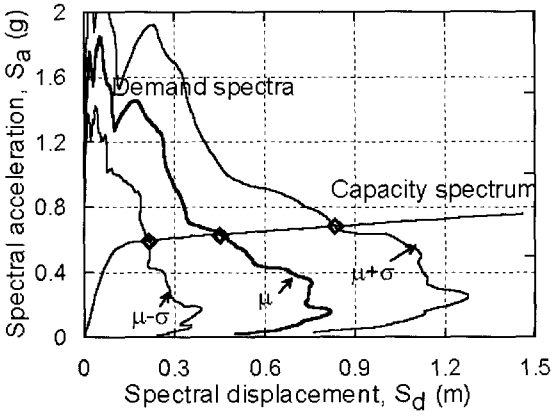

(d) Representative PGA=0.8g

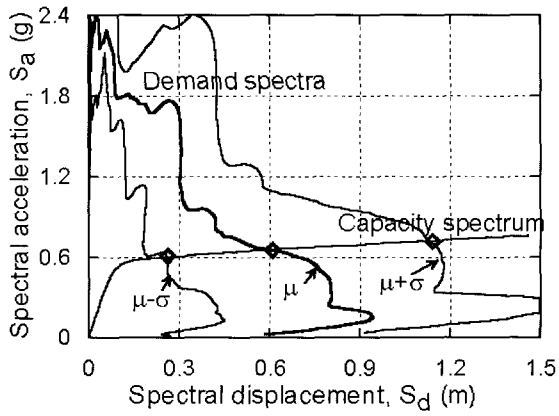

(e) Representative PGA=1.0g

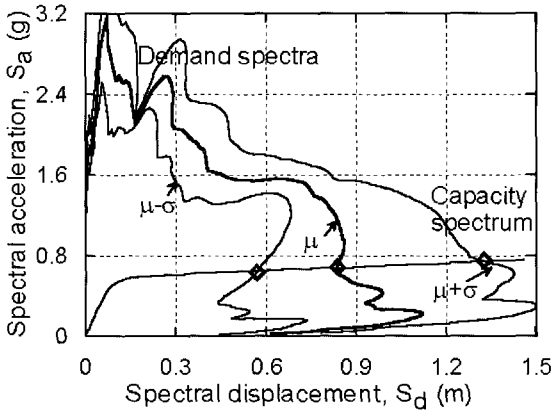

(f) Representative PGA=1.2g

Table 8 Spectral displacements and statistical properties for each representative PGA values(CSM1)PGA

the fragility curves not to intersect, can also be estimated. The likelihood formulation described by Shinozuka et al.[8] is used for the purpose of this method.

4.2 Fragility Curves by CSM

The CSM is considered as much a simplified procedure as possible in evaluating bridge response using a code-type predetermined response spectrum rather than an individual spectrum associated with a particular ground motion time history. The most appropriate approach to develop fragility curves using CSM, four(4) methods are introduced in Table 7. CSM1 and CSM2 were studied by the authors (Shinozuka et al 2000), while CSM3 and CSM4 are developed

Table 7 Four (4) different approaches in developing demand spectrum for CSM

Names	Sixty(60) ground motion time histories	Reduction factors
CSM1	Six(6) grouped spectrums by scaling	Yes
CSM2	Six(6) grouped spectrums by scaling	No
CSM3	Sixty(60) individual spectrums	Yes
CSM4	Sixty(60) individual spectrums	No

to examine the improvement of the method presented in this study.

For CSM1 and CSM2, ground motion time histories are sorted by PGA and grouped to the nearest representative PGA(e.g. 0.20, 0.45, 0.60, 0.8, 1.0, 1.2) by scaling as in Table 4. For each group of PGA, the mean and standard deviation of the elastic acceleration response spectra for all the time histories in the group are calculated for the range of structural period considered. By developing three elastic acceleration response spectra in this way(i.e., mean and meanone standard deviation) and transforming them to ADRS format, three ADRS, i.e., mean (μ) and meanone standard deviation ($\mu \pm \sigma$) ADRS, are developed. Then a capacity spectrum for the sample bridge is constructed and drawn on the same coordinates. The three performance points for each of the capacity spectrum are determined as its intersections with μ and $\mu \pm \sigma$ ADRS. These three spectral displacements are defined as $S_d^0(a)$ and $S_d^{\pm} = S_d^0(a) \pm \sigma_d(a)$ and shown in Figs. 7 and 8 for the CSM1 and CSM2 in Table 7, respectively. Since the three ADRS are developed on the time histories grouped by PGA, they are functions of a(PGA).

It is assumed that the spectral displacement has the mean $S_d^0(a)$ and the standard deviation $\sigma_d(a)$ defined as $\sqrt{\sigma_d^+(a) \cdot \sigma_d^-(a)}$. The two parameters are obtained from the following equations under the assumption that the spectral displacement can be expressed as lognormal distribution listed in Tables 8 and 9 for CSM1 and CSM2, respectively.

$$\overline{S}_d(a) = c(a)\exp[\{\zeta(a)\}^2/2] \tag{10}$$

$$\{\sigma_d(a)\}^2 = \{\overline{S}_d(a)\}^2[\exp(\{\zeta(a)\}^2) - 1] \tag{11}$$

$S_d^0(a)$ and $S_d^{\pm} = S_d^0(a) \pm \sigma_d(a)$ of the sample bridge for each PGA are also shown in Fig. 9 for CSM1 and CSM2.

The limit displacement d_l defined as the spectral displacement $S_d(a)$ for the specified state of damage can be obtained from (12)

$$d_l = \frac{\theta_{pl}/\theta_y}{PF\phi_{pl}/\theta_y} = \frac{Ductility\ Demand)_{damage}}{(PF\phi_{pl})_{damage}/\theta_y} \tag{12}$$

where $(X)_{damage}$ denotes the value of X at the specified state of damage and θ_y is the yielding rotation of the plastic hinge. In general, the probability that sample bridge j will have a state of damage exceeding d_l is given by

$$P[S_d(a) \geq d_l \text{ for sample bridge}] = P(a, d_l) = 1 - \Phi\left[\frac{\ln(d_l/c(a))}{\zeta(a)}\right] \tag{13}$$

Table 8 Spectral displacements and statistical properties for each representative PGA values(CSM1)PGA

PGA	$S_d^0(a)$	$S_d^-(a)$	$S_d^+(a)$	c(a)	$\zeta(a)$
0.2	0.0530	0.0445	0.0615	0.0523	0.1588
0.4	0.0784	0.0665	0.1121	0.0760	0.2511
0.6	0.1256	0.0735	0.2958	0.1005	0.6678
0.8	0.2113	0.1262	0.3728	0.1848	0.5179
1.0	0.2789	0.1247	0.5643	0.2229	0.6695
1.2	0.5737	0.4349	0.8164	0.5464	0.3121

Table 9 Spectral displacements and statistical properties for each representative PGA values(CSM2)PGA

PGA	$S_d^0(a)$	$S_d^-(a)$	$S_d^+(a)$	c(a)	$\zeta(a)$
0.2	0.0530	0.0445	0.0615	0.0523	0.1588
0.4	0.1529	0.0732	0.2878	0.1266	0.6151
0.6	0.3259	0.1507	0.5472	0.2789	0.5578
0.8	0.4588	0.2174	0.8343	0.3836	0.5984
1.0	0.6122	0.2615	1.1355	0.5016	0.6313
1.2	0.8370	0.5724	1.3327	0.7682	0.4142

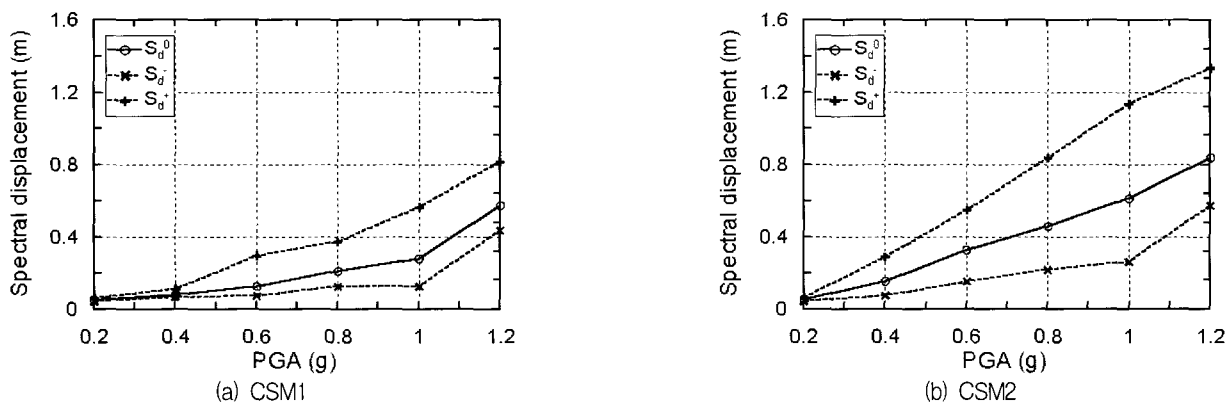

(a) CSM1 (b) CSM2

Fig. 9 Performance displacement of sample bridge

where $d_l=(d_l)_1$, $d_l=(d_l)_2$, $d_l=(d_l)_3$, $d_l=(d_l)_4$ and $d_l=(d_l)_5$ represent respectively the states of almost no, slight, moderate, extensive and collapse damage under the assumption that the same state of damage will be imposed on all the columns simultaneously as the nonlinear static analysis tends to imply.

For CSM3 and CSM4, each of sixty(60) ground motion time histories in Table 7 is considered as a single event and nonlinear static procedure is performed for each event to evaluate damage states of columns of the sample bridge. Then, fragility curves are represented by lognormal distribution functions with two parameters as a function of peak ground acceleration(PGA).

The maximum horizontal displacement of the girder and the maximum rotational displacement at column bottoms by CSM3, CSM4 and NTHA(Nonlinear Time History Analysis) are examined. The response ratios, defined as the "response by the CSM" divided by the "response by the NTHA", are plotted as a function of the ductility demand for plastic hinge as shown in Fig. 10. For the maximum horizontal displacement of the girder, the responses by CSM3 and CSM4 are almost same as that from NTHA up to ductility of 2.0, while they show considerably greater displacements than the time history analysis after this range. For ductility between 4.0 and 5.0, the difference in the response by two methods increases three times for CSM3 and six times for CSM4, respectively, as shown in Fig. 10(a). Fig. 10(b) also shows a similar trend except that the responses by CSM3 become smaller for the ductility demands between 2.0 and 11.0.

Fragility curves for the sample bridge associated with those damage states are developed and plotted in Fig. 11 for the cases CSM1, CSM2, CSM3, CSM4 and NTHA as a function of PGA.

Considering five(5) case fragility curves, the fragility curves by CSM3 and 4 are rather consistent than those by CSM1 and 2 in comparing with the one by NTHA. It is noted that CSM1 and 2 might loose their original characteristics of earthquake ground motions by grouping and scaling of ground motion time histories and result in different responses from those by NTHA.

5. Discussions and Conclusions

This study examines the fragility curves of the sample bridge by four(4) different analytical approaches utilizing CSM, and the results are compared with those by the time history analysis. The comparison indicates that the CSM4 is a best approach showing excellent agreement for all the damage states, while the others do show discrepancy at more severe states of damage where nonlinear effects obviously play a crucial role.

The following conclusions are drawn from the results of this study, however, this observation might not always apply, depending on the details of specific bridge characteristic.

(1) Grouping and scaling of ground motion time histories might loose their original characteristics of earthquake ground motions resulting in different responses from those by time history analysis (CSM1&2 vs CSM3&4).
(2) Horizontal displacements of the bridge girder with reduction factors produces similar responses with those by time history analysis, while rotational displacements at column bottom without reduction factors do overall (CSM1&3 vs CSM2&4).
(3) Although CSM4 is a best fit in applying CSM to develop fragility curves of the sample bridge, CSM2 might be better for the purpose of practical use.

Acknowledgement

The second writer is grateful for the support by the Korea Science and Engineering Foundation as a postdoctoral fellow.

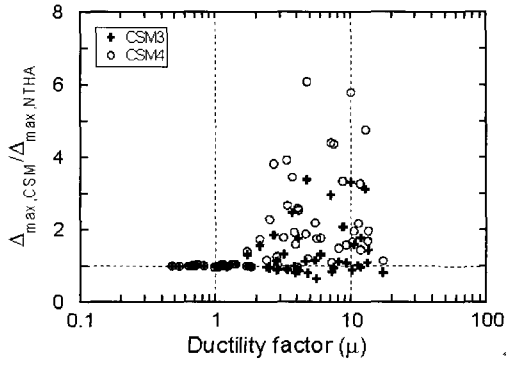

(a) Horizontal displacements of bridge girder

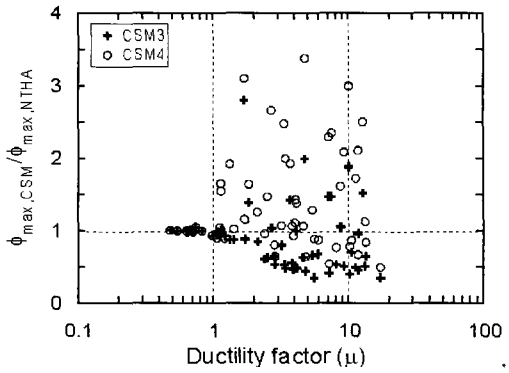

(b) Rotational displacements at column bottoms

Fig. 10 Response ratios of sample bridge as function of ductility demand

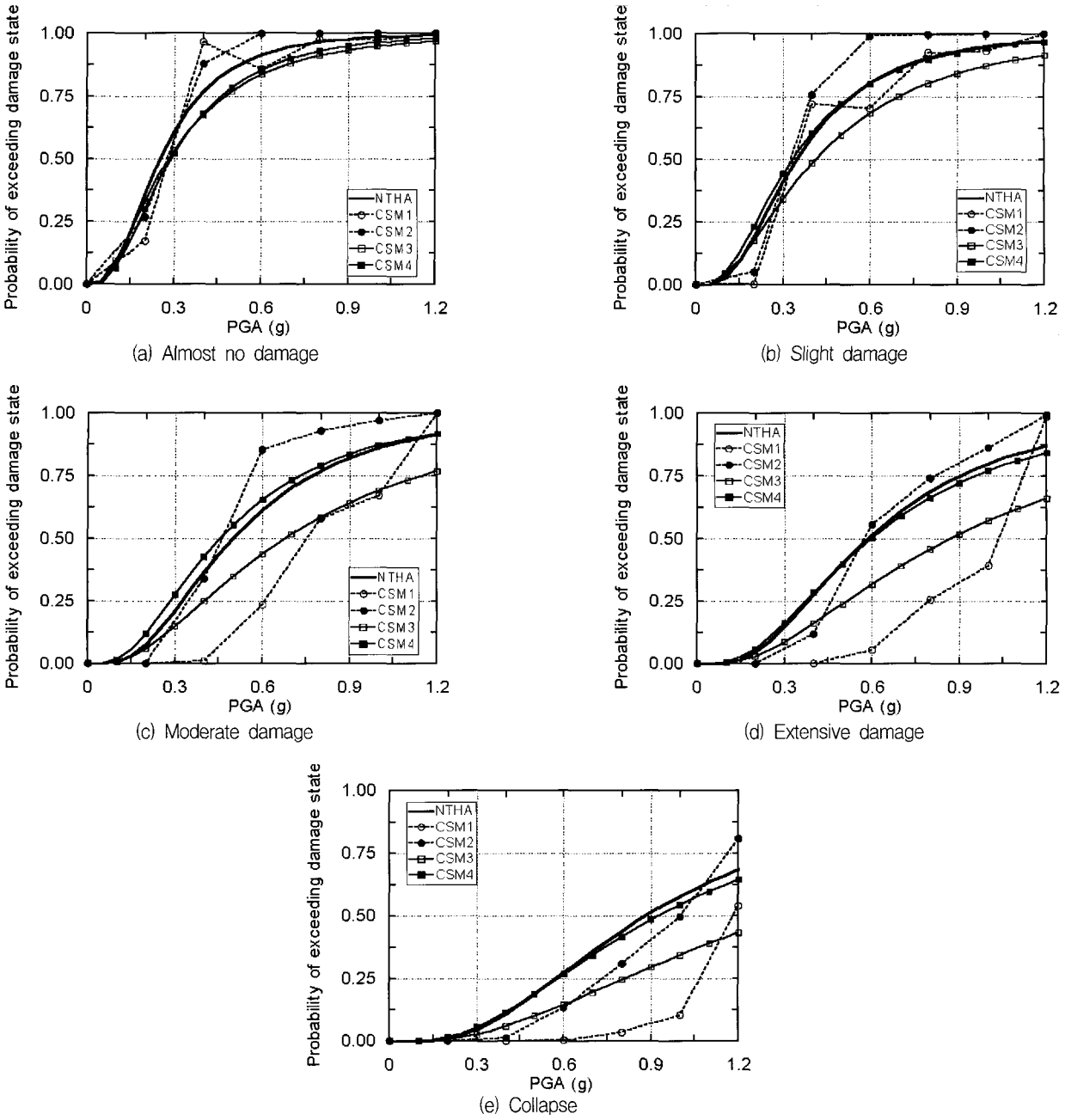

(a) Almost no damage

(b) Slight damage

(c) Moderate damage

(d) Extensive damage

(e) Collapse

Fig. 11 Fragility curves of sample bridge

References

1. Dutta, A., "On energy based seismic analysis and design of highway bridges," Ph. D. Dissertation, Dept. of Civ., Struct. & Envir. Engrg., State University of New York at Buffalo, Buffalo, NY, 1999.
2. Barron, R., "Spectral Evaluation of Seismic Fragility of Structures," Draft of Ph.D. Dissertation, Dept. of Civ., Struct. & Envir. Engrg., State University of New York at Buffalo, Buffalo, NY, 2000.
3. Shinozuka, M., Feng, M. Q., Kim, H., and Kim, S., "Nonlinear Static Procedure for Fragility Curve Development," *Journal of Engineering Mechanics*, ASCE, Vol. 12, No. 12, 2000, pp. 1287-1295.
4. Applied Technology Council(ATC), "Seismic Evaluation and Retrofit of Concrete Buildings," *Rep. No. SSC 96-01*: ATC-40, 1, Redwood City, CA, 1996.
5. Federal Emergency Management Agency(FEMA),. "NEHRP Guidelines for the Seismic Rehabilitation of Buildings," *FEMA-273*, Washington, D.C., 1997.
6. City of Los Angeles(COLA), "Earthquake Hazard Reduction in Existing Reinforced Concrete Buildings and Concrete Frame Buildings with Masonry Infills," Los Angeles, CA, 1995.
7. California Department of Transportation, *COLx Users Manual*, Sacramento, CA, 1993.
8. Shinozuka, M., Feng, M. Q., Kim, H., Uzawa, T., and Ueda, T., "Statistical Analysis of Fragility Curves," Multidisciplinary Center for Earthquake Engineering Research, *Technical Report*, 2003.